Structure of Highly Sheared Tropical Storm Chantal during CAMEX-4

G. M. HEYMSFIELD,* J. HALVERSON,+ E. RITCHIE,# JOANNE SIMPSON,* J. MOLINARI,@ AND L. TIAN+

*NASA Goddard Space Flight Center, Greenbelt, Maryland
+University of Maryland, Baltimore County, Baltimore, Maryland
#University of New Mexico, Albuquerque, New Mexico
@Department of Earth and Atmospheric Sciences, University at Albany, State University of New York, Albany, New York

(Manuscript received 16 October 2003, in final form 21 December 2004)

ABSTRACT

Tropical Storm Chantal during August 2001 was a storm that failed to intensify over the few days prior to making landfall on the Yucatan Peninsula. An observational study of Tropical Storm Chantal is presented using a diverse dataset including remote and in situ measurements from the NASA ER-2 and DC-8 and the NOAA WP-3D N42RF aircraft and satellite. The authors discuss the storm structure from the larger-scale environment down to the convective scale. Large vertical shear (850–200-hPa shear magnitude range 8–15 m s^{-1}) plays a very important role in preventing Chantal from intensifying. The storm had a poorly defined vortex that only extended up to 5–6-km altitude, and an adjacent intense convective region that comprised a mesoscale convective system (MCS). The entire low-level circulation center was in the rain-free western side of the storm, about 80 km to the west-southwest of the MCS. The MCS appears to have been primarily the result of intense convergence between large-scale, low-level easterly flow with embedded downdrafts, and the cyclonic vortex flow. The individual cells in the MCS such as cell 2 during the period of the observations were extremely intense, with reflectivity core diameters of 10 km and peak updrafts exceeding 20 m s^{-1}. Associated with this MCS were two broad subsidence (warm) regions, both of which had portions over the vortex. The first layer near 700 hPa was directly above the vortex and covered most of it. The second layer near 500 hPa was along the forward and right flanks of cell 2 and undercut the anvil divergence region above. There was not much resemblance of these subsidence layers to typical upper-level warm cores in hurricanes that are necessary to support strong surface winds and a low central pressure. The observations are compared to previous studies of weakly sheared storms and modeling studies of shear effects and intensification.

The configuration of the convective updrafts, low-level circulation, and lack of vertical coherence between the upper- and lower-level warming regions likely inhibited intensification of Chantal. This configuration is consistent with modeled vortices in sheared environments, which suggest the strongest convection and rain in the downshear left quadrant of the storm, and subsidence in the upshear right quadrant. The vertical shear profile is, however, different from what was assumed in previous modeling in that the winds are strongest in the lowest levels and the deep tropospheric vertical shear is on the order of 10–12 m s^{-1}.

1. Introduction

Observational studies have generally found that large-scale vertical shear is unfavorable for tropical storm formation and intensification (e.g., Gray 1968; Zehr 2003). The vertical shear that affects tropical storm intensity is the environmental shear defined as the difference between the 200- and 850-hPa winds averaged over a large area centered on the storm (e.g., DeMaria 1996). All storms have some amount of shear and why certain storms intensify is a fundamental question in hurricane research. Numerical modeling studies have suggested the primary mechanism forcing wavenumber-1 asymmetries in rainfall distributions is vertical shear (e.g., Frank and Ritchie 2001; Bender 1997; Jones 1995). Frank and Ritchie (2001) hypothesized that a large-scale shear imposed on a storm can cause high values of potential vorticity and equivalent potential temperature (θ_e) to mix outward rather than into the eye. This results in a loss of the upper tropospheric warm core in the eye and would tend to weaken the storm by increasing the central pressure. Frank and

Corresponding author address: Gerald M. Heymsfield, NASA GSFC, Code 613.1, Greenbelt, MD 20771.
E-mail: Gerald.heymsfield@nasa.gov

Ritchie (1999) found that in moist simulations, shear-induced vertical velocity dipoles occur through a deep portion of the troposphere such that maximum upward motions occur in the downshear left quadrant and subsidence occurs in the upshear right quadrant. Rogers et al. (2003) studied the effects of vertical shear on asymmetries in low-level convergence, vortex tilt, and rainfall in Hurricane Bonnie. They found that the distribution of model-derived radar reflectivity was closely related to the vertical shear vector magnitude and direction.

In support of the secondary circulation structure suggested by models, observations have shown that strong wavenumber-1 asymmetries occur in rainfall and vertical velocity fields with the maximum rainfall occurring on the left side of the shear vector (Marks et al. 1992; Franklin et al. 1993). Black et al. (2002) presented an observational study on the interactions of vertical shear on two hurricanes: Jimena (1991) and Olivia (1994). While the initial intensity and structure of these storms were similar, Olivia intensified whereas Jimena did not. In both storms, shear controlled the convective structure and shears greater than 8 m s^{-1} produced a wavenumber-1 distribution of convection. Highest reflectivities formed to the left of the shear vector and most radar echoes and updrafts were located in the downshear quadrant of the storm and rotated around the eye, consistent with Rossby vortex wave propagation. Olivia was an example of a hurricane that weakened rapidly after development of an intense convective cells or supercells on the north side. Vertical shears of 10 m s^{-1} in observational studies (e.g., Zehr 1992) and 10–15 m s^{-1} in modeling studies (e.g., Frank and Ritchie 2001) have resulted in adverse effects on storm intensity; the latter modeling study found that a 15 m s^{-1} shear would tear an intense storm apart in about a day. It is clear that improvements in tropical storm intensity forecasting depend in part on how well we understand the response of tropical cyclones to environmental vertical shear. Shear not only affects vertical motions in tropical storms, but there is also evidence that it similarly affects midtropospheric cyclonic vortices (MCVs) associated with MCSs. Trier et al. (2000) studied observational and modeling aspects of a land-based MCS with an MCV experiencing vertical wind shear and they found the same downshear left maximum upward motions. Recent papers by Corbosiero and Molinari (2002) note that tropical depressions, storms, and hurricanes all display the identical lightning signature with respect to vertical wind shear, that is, a strong preference for convection downshear left in the inner core region. Therefore, the vertical motion location relative to a vortex embedded in sheared flow appears to occur all the way from midlevel vortices over land and water to full-fledged hurricanes.

While shear has been linked to the changes in intensity of tropical storms, the role of inner core convection on storm intensification has been the subject of numerous studies. Observationally, sudden intensification has been linked to the occurrence of convective bursts that are intense, long-lived ensembles of deep convection topped by an anomalously cold infrared (IR) anvil cloud mass covering an area larger than the meso-γ scale (Gentry et al. 1970; Holliday and Thompson 1979; Steranka et al. 1986; Ritchie et al. 2003). The convective towers, commonly referred to as hot towers, carry high θ_e air aloft and detrain this air into the eye leading to warming of the inner core and lowering of the central pressure (Malkus and Riehl 1960; Simpson et al. 1998). Some of these hot towers may be exceptionally vigorous and overshoot their equilibrium level. A recent example of hot towers in an intensifying hurricane is in the paper by Heymsfield et al. (2001), which examined the internal structure of a convective burst and its relationship to the warm core during Hurricane Bonnie's intensification, using a synthesis of high- resolution satellite, aircraft radar, and in situ data. An exceptionally vigorous eyewall tower within the burst penetrated to nearly 18 km and high θ_e air detrained from the burst subsided within Bonnie's eye, and it was speculated that this might provide favorable warming for storm intensification.

Modeling studies have shown that the dynamic response to intense bursts of convection and mesoscale convective systems in the inner core of tropical cyclones is the development of discrete vortices that then mix into the vorticity core of the tropical cyclone, resulting in intensification (e.g., Ritchie and Holland 1997; Montgomery and Enagonio 1998; Ritchie et al. 2003). Such processes were concluded to be occurring in the genesis and eye formation processes in Tropical Cyclone Oliver (1993) (Simpson et al. 1997) and Hurricane Floyd (1999) (Ritchie et al. 2003).

One of the observational difficulties in examining the vortex response to shear and the role of convection in hurricane intensification is that it requires detailed knowledge of multiple scales ranging from the larger-scale storm environment, the vortex scale, down to individual convective elements. This is alluded to in Stossmeister and Barnes (1992, hereafter SB92), who documented the development of a second vortex in Tropical Storm Isabel that evolved into the circulation center of the storm. The new circulation center developed outside of the radius of maximum wind in a rain-free region and was associated with convection ~90 km to the northwest of the original center. While warm

cores and θ_e in hurricanes are generally found at the circulation center, SB92 found the new circulation center initially developed below anvil in a region of low θ_e ~346 K very warm air that was suggestive of subsidence. Eventually, θ_e increased to 360 K, which is more typical of hurricane warm cores. They suggested that models may be missing an important step since high θ_e is usually assumed in the core at all times. The SB92 concept of the initial development of a vortex is somewhat different than other theories that consider warm core and cyclonic vortex development in stratiform regions. For example, Raymond and Jiang (1990) suggested that the vertical gradient of diabatic heating due to latent heating in a stratiform cloud and evaporative cooling below cloud base may concentrate cyclonic potential vorticity (PV) at midtropospheric levels that may result in the formation of midlevel vortices. Ritchie and Holland (1997) and Bister and Emanuel (1997) suggested that midlevel MCVs are a necessary precursor for tropical cyclogenesis and that with these top-down mechanisms, a vortex develops downward to lower levels.

The Wind-Induced Surface Heat Exchange (WISHE) instability first suggested by Emanuel (1986) is one formal theory for intensification of tropical cyclones. This theory essentially suggests that a wind field can amplify purely from the surface moist entropy flux. Molinari et al. (2004, 2006) have examined Tropical Storm Gabrielle (2001) and Hurricane Danny (1997) in terms of WISHE theory. For Hurricane Danny, they found that few of the WISHE assumptions were met in the tropical depression and early tropical storm periods, but that WISHE intensification occurred later in the storm lifetime when a single near-axisymmetric vortex was present on the ocean surface, and convection moistened midlevels to create a more slantwise neutral sounding. Molinari et al. (2006) suggested that Gabrielle did not intensify into a hurricane since very dry lower tropospheric air upshear of the vortex was drawn into the circulation, and the WISHE assumptions were not met since this dry air helped prevent a tight coupling between ocean surface fluxes, convection, and surface winds.

During the 2001 Atlantic hurricane season, National Aeronautics and Space Administration (NASA) and National Oceanic and Atmospheric Administration (NOAA) conducted an extensive field campaign to study hurricanes on multiple scales and covering multiple objectives (Hood et al. 2006). NASA's component, the Fourth Convection and Moisture Experiment (CAMEX-4), combined with an enhancement of NOAA's Hurricane Field Program (HFP 2001), resulted in an unprecedented study of hurricanes from the upper levels of the atmosphere (NASA aircraft) through the middle levels of the atmosphere (NASA and NOAA aircraft) to the boundary layer (NOAA aircraft).

In light of the previous observations on the role of vertical shear and convective bursts on storm intensification, we examine Tropical Storm Chantal during CAMEX-4 that had very intense convection but failed to intensify in moderate to strong environmental shear. On 20 August 2001, the NASA high-altitude (20 km) ER-2 and medium-altitude (9–12 km) DC-8 aircraft, and the lower-altitude (3–6 km) NOAA N42RF, conducted a coordinated Quantitative Precipitation Estimation (QPE) mission focused on a strong region of convection close to Tropical Storm Chantal's low-level center of circulation (Black et al. 2001). The NASA (ER-2 and DC-8) and NOAA WP-3D (N42RF) aircraft based at Jacksonville and Tampa, Florida, respectively, flew east of the Yucatan–Belize coast for this mission. An intense convective burst episode was occurring during the aircraft flights, and the ER-2 and DC-8 were stacked close in time and location, with the ER-2 over the top of the burst and the DC-8 penetrating it. The NASA aircraft collected remote sensing (radar, radiometer), in situ, and dropsonde datasets, while the N42RF collected radar, in situ, and dropsonde data at lower levels. The ER-2 and DC-8 were each instrumented with down-looking radars called ER-2 Doppler radar (EDOP; Heymsfield et al. 1996) and the DC-8 precipitation radar-2 (PR-2; Sadowy et al. 2003) as well as other instruments described elsewhere in this special issue. EDOP, a focus in this paper, is a fixed dual-beam X-band radar (nadir and forward-looking beams) from which vertical and along-track horizontal winds can be calculated (Heymsfield et al. 1996).

There are several objectives of this paper: 1) to analyze the mesoscale structure of a nondeveloping tropical storm from the surface through various upper levels to illustrate the relationship of Chantal's intense convection (a convective burst) to the low-level vortex, winds, and moisture, the tropospheric warm anomaly, and the tropospheric shear using a synthesis of N42RF and DC-8 flight-level data, dropsondes, and satellite [Geostationary Operational Environmental Satellite (GOES) and Tropical Rainfall Measuring Mission (TRMM) Microwave Imager (TMI)] information; and 2) to use the analyzed fields in 1) as a mesoscale context to examine the convective-scale features of the burst, that is, updraft/downdraft structure, reflectivities, and θ_e using the high-resolution two-dimensional ER-2 Doppler radar measurements. This focus will help to understand why Chantal's intense burst was sustained

to the east-northeast of the vortex for such a long time. Our observations will be compared with other observations to help understand why Chantal did not intensify.

2. Large-scale storm environment and convective burst evolution

Chantal first became a depression on 14 August, a weak tropical storm on 17 August, and it weakened slightly early on 20 August and reintensified later in the day just prior to landfall. The storm was forecast to intensify early on 20 August and eventually made landfall near the Yucatan–Belize border early on 21 August (Fig. 1). The minimum sea level pressures (MSLP) ranged from 1005 to 1006 hPa on 18 August to a minimum of 994 hPa at 12 UTC on 19 August, to 1006–1007 hPa late on 20 August (Figs. 1 and 2a). The maximum surface winds (MSWs) increased from ~25 to 30 m s^{-1} early 19 August, and then fluctuated from 28–30 m s^{-1} until landfall early on 21 August (Fig. 2a). Chantal's movement was west-northwest (255°–285°) from 18–20 August, and its speed continually decreased from a peak of 12 m s^{-1} late on 18 August, to about 4 m s^{-1} near landfall (Fig. 2b).

Since the soundings were very sparse in Chantal's environment, the 200–850-hPa vertical shear during this period was calculated based on the National Centers for Environmental Prediction (NCEP) Global Tropospheric Analyses, which are 1° global analyses based on the Global Forecast System (GFS formerly AVN) but with a synoptic time +6 h cutoff so more data makes it into the analysis. The horizontal winds were averaged

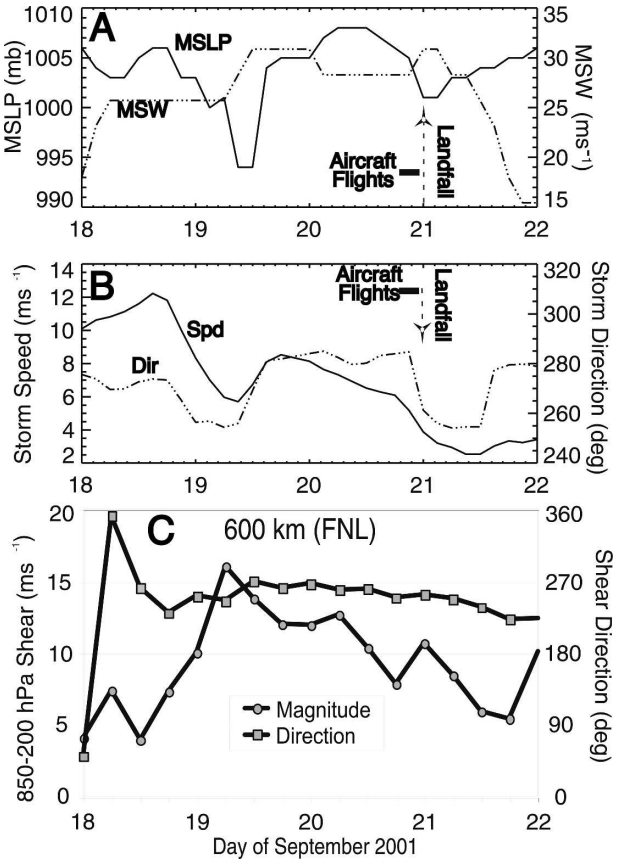

FIG. 2. History of Tropical Storm Chantal from 18 to 22 Aug. (a) MSLP and MSW traces, (b) storm advection speed and direction, and (c) model-calculated vertical shear magnitude and direction from NCEP analyses. See text for details.

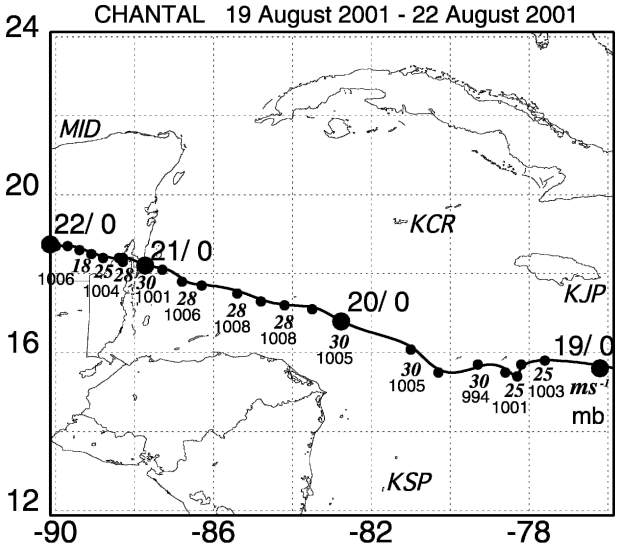

FIG. 1. Tropical Storm Chantal best track. Minimum mean sea level pressure (MSLP; in hPa), and maximum surface winds (MSW; in m s^{-1}) are shown at 3-h intervals.

at the 850- and 200-hPa levels over a 600-km radius centered on the National Hurricane Center's (NHC) best-track position, and shear was calculated from the difference between the winds at the two levels (Fig. 2c). The plot shows a distinct shear minimum (<5 m s^{-1}) on 1200 UTC 18 August, and Chantal appears to intensify to its lowest central pressure (994 hPa) during the subsequent 18–24 h. During this intensification period, the shear magnitude increased and became strong (>10 m s^{-1}) from 0000 UTC 19 August until about 1200 UTC 20 August. The shear peaked (>15 m s^{-1}) at 0600 UTC 19 August near the time when Chantal achieved its lowest central pressure, and after this peak the shear decreased with local minima at 1800 UTC 20 August and 1800 UTC 21 August. Given that Chantal appeared to be intensifying through this period, the high shear magnitudes are very surprising, but it suggests the storm takes time to respond to shear, which has been modeled by Frank and Ritchie (2001) and observed by Gallina and Velden (2000). The shear direction is gen-

erally 260°–270° from 1200 UTC 19 August to 1200 UTC 20 August, and then backs 45° over the next 36 h.

The general precipitation structure associated with Chantal is depicted in Fig. 3 with the GOES visible and 10.8-μm IR image at 2002 UTC 20 August, and the TMI 85-GHz temperatures at 2034 UTC. The approximate location of Chantal's low-level center of circulation is shown west-southwest of an intense convection region that produced cold IR (~193 K) and 85-GHz temperatures (~126 K; Figs. 3b,c, respectively). This region is representative both in location relative to the circulation center and intensity of the convective activity associated with Chantal on 19–20 August.

Since Chantal was located far from the NASA and NOAA aircraft bases and the NASA aircraft were not authorized to fly over Mexico, it was decided to focus on the heavy rain region over water in the right-rear quadrant of Chantal. Flight planning by NOAA and NASA scientists allowed for excellent coordination between the aircraft. On several passes, the ER-2, DC-8, and N42RF when possible because of their lower airspeed, were stacked vertically. The DC-8 and ER-2 performed three main passes across the storm (labeled 1–3 in Fig. 3b). The DC-8 experienced severe icing during the first flight leg (Herman and Heymsfield 2003) that required its descent to lower altitudes from a nominal 12-km altitude, and a diversion around cell 2 during pass 2. After passes 1–3, the aircraft then focused on the heavy convective rainband farther northeast of the core of cell 2. The N42RF performed shorter passes, sometimes coordinated with the ER-2 and DC-8 (Fig. 3c), at other times focused on flight legs for Doppler analysis.

The general state of the surface conditions that Chantal encountered were obtained from TRMM TMI–derived SST (Fig. 4a) and the Quick Scatterometer (QuikSCAT)-derived surface winds (Fig. 4b). QuikSCAT and TRMM did not have useful passes on 20 August, so 19 August is presented since the main interest here is in the larger-scale conditions that do not change rapidly. The QuikSCAT pass is from 19 August and the TRMM microwave-derived SST is based on a 3-day average (18–20 August) centered on 19 August based on the standard TRMM algorithms (Wentz et al. 2000). Also shown are GOES IR contours at 200 and 240 K from 0000 UTC on 20 August that represent an outline of Chantal's cirrus outflow near the time of the QuikSCAT data. From the SSTs and Chantal's west-northwest motion, it is evident that Chantal moved into slightly warmer (30°C) water on 20 August from ~28° farther east a day earlier. The surface winds obtained from the Jet Propulsion Laboratory (JPL) level 2B wind product (QuikSCAT 2001) were strong easterlies with a large curvature north of the Chantal's precipita-

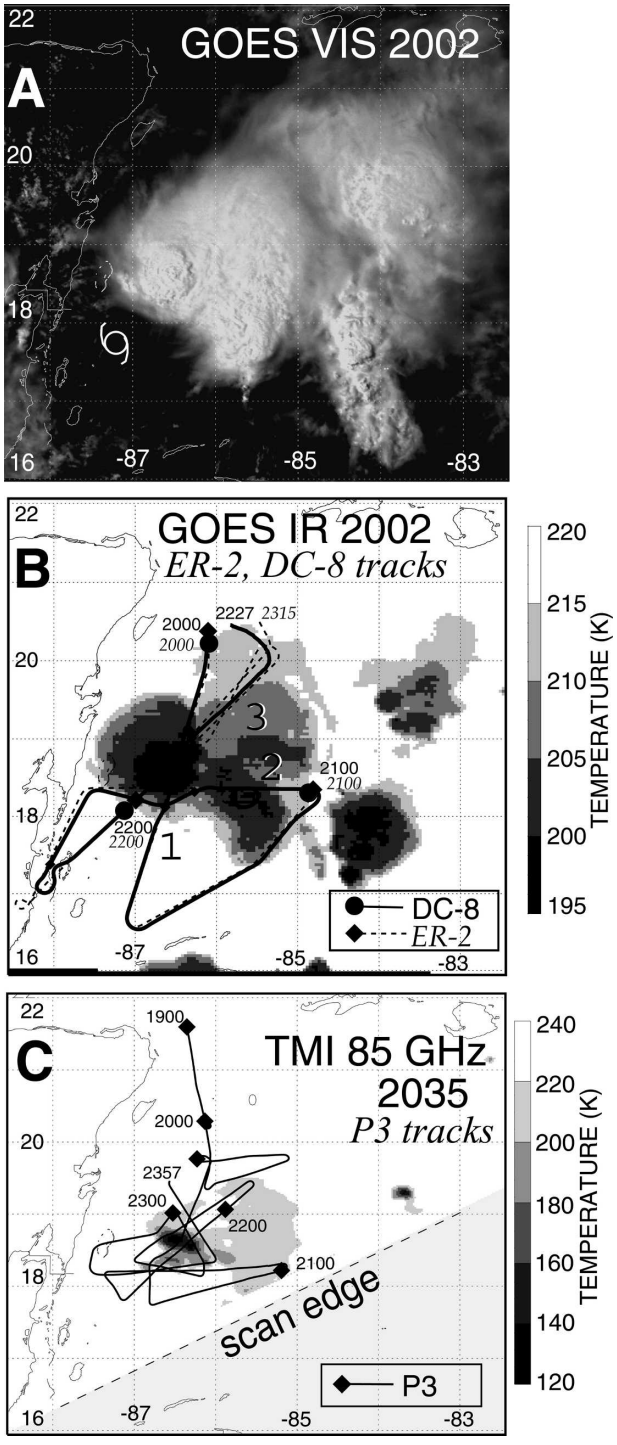

FIG. 3. Satellite images from GOES and TRMM on 20 Aug 2001. (a) GOES visible image at 2002 UTC, (b) GOES IR 10.8-μm image at 2002 UTC, and (c) TRMM TMI 85-GHz image at 2034 UTC. The edge of the TRMM swath is noted on the lower half of (c). The ER-2 and DC-8 flight tracks are superimposed on (b), and the N42RF flight track is shown in (c). ER-2 and DC-8 passes 1–3 are indicated in (b). Grid lines are in 1° intervals.

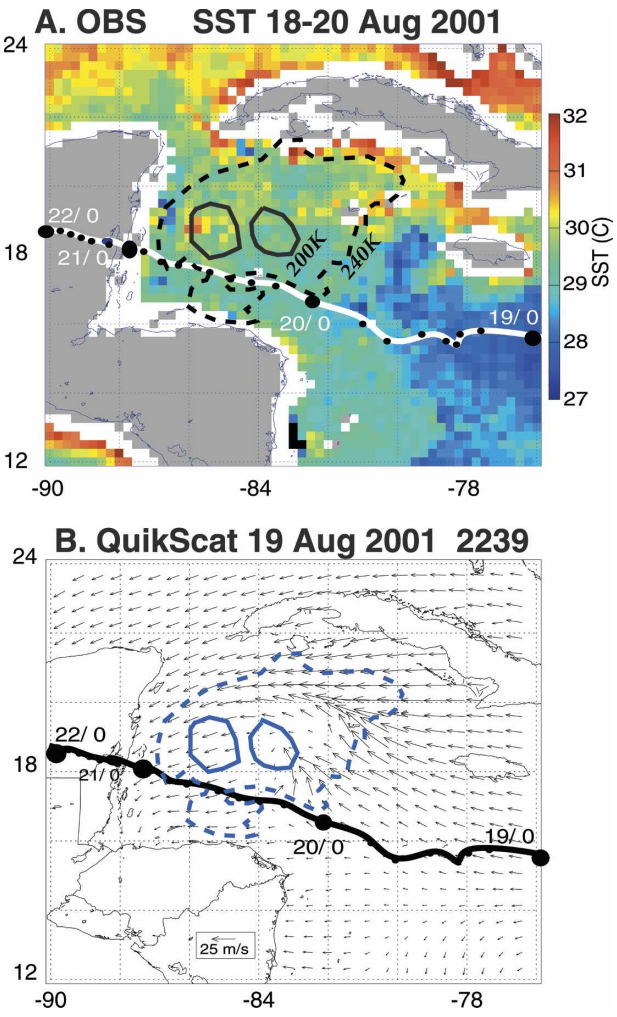

FIG. 4. Large-scale surface conditions. (a) Three-day-averaged SSTs derived from TMI. (b) Surface winds derived from the QuikSCAT level 2b product. Chantal's track is superimposed on both panels and 200-K (solid) and 240-K (dashed) IR brightness temperature contours are provided for reference.

tion region and weak easterlies to the south of the storm track. Strong mesoscale confluence is noted on the east-northeast portion of the storm, which provides forcing for the convection as will be discussed later in section 4. There is not a well-defined circulation in the winds that is likely due to inability of the satellite-derived winds to capture Chantal's small low-level circulations (LLCs). QuikSCAT has 25-km resolution and the wind direction can be greatly affected by the heavy rain in Chantal's precipitation region.

The synoptic-scale vertical structure associated with Chantal is best depicted through a combination of conventional soundings and forecast model winds. Figures 5a–c show 1200 UTC soundings from west to east across the region shown in Fig. 1 [Mérida, Mexico (MID); Grand Cayman (KCR); and Kingston, Jamaica (KJP)]. These soundings were north of the storm track and there were no soundings south of the storm track on 20 August. The storm environment horizontal winds and vertical wind shear vector derived from the 1200 UTC 20 August NCEP final analysis is shown in Fig. 5d. The soundings show strong large-scale, zonal-reversing flow with low-level easterly flow 10–20 m s^{-1} up to about 6-km altitude, and southwesterly flow 10–20 m s^{-1} in the upper troposphere (>9 km altitude). The averaged model-derived storm environment winds have lower magnitudes with ~8 m s^{-1} low-level easterly flow and 4 m s^{-1} westerly flow near 200 hPa. Part of this model–observation difference is the inability of the NCEP final analysis to capture mesoscale details of the storm and part is the effects of averaging, which will tend to reduce observed peak values. Also, the observed winds are stronger on the north side of Chantal, and there were few soundings on the south side of the storm where weaker values would be located. Chantal's motion is mostly toward the west (~6 m s^{-1}), so the storm-relative winds are very weak. The NCEP fields did not include the research sondes that would have been quite helpful in this data-sparse region.

Figure 6 shows a sequence of color-enhanced GOES cloud-top temperatures covering the aircraft flights 2002–2332 UTC on 20 August. A strong convective burst that consists of several large cells occurs during this image sequence. A first strong cell (cell 1) developed prior to 2002 UTC. Then a second cell (cell 2; 18.6°N, 86.7°W) is evident in Figs. 6a,b developed ~80 km to the northwest of cell 1. Finally, another very strong cell (cell 3) developed ~80 km farther to the west of the cell 2 remnants about 3 h later at 2302 UTC. Cell 2 was the dominant cell and it rapidly developed both with lowered cloud-top temperatures and an expanding anvil (dashed lines in Fig. 6) over a 2-h period. Convective activity 12–18 h prior to this burst episode was sporadic with occasional strong cells, none of which produced rapid anvil expansion as shown in Fig. 6. In general though, smaller bursts were continually redeveloping in at least two main regions, often separated by 100–200 km and located to the east-northeast of the low-level circulation center. These intense bursts evolved in the IR imagery from cold, overshooting tops, to expanding anvils, to dissipation, over a few hours. The rapid expansion of the temperature contours in Fig. 6 imply strong upward mass fluxes produced by cells during this period. The cells moved to the west with the storm center rather than being formed by a relatively fixed area of overshooting hot towers. The contribution of individual cells to forming a larger-scale burst is similar to the succession of cells that formed in

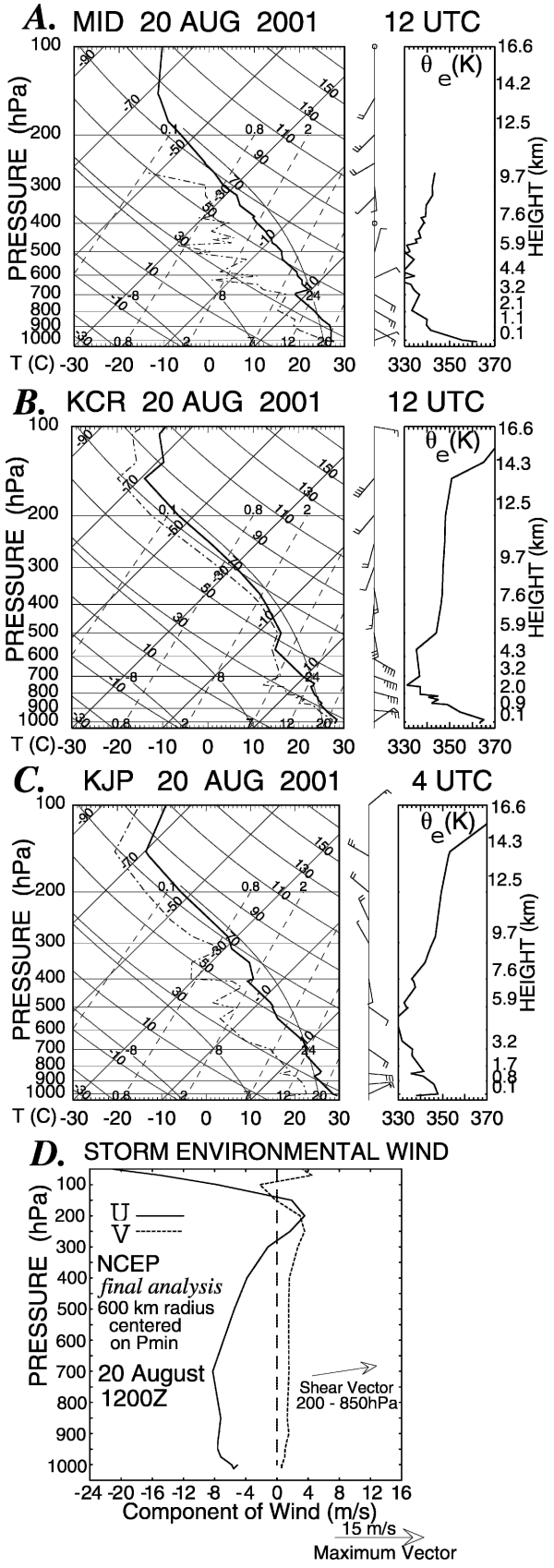

←

FIG. 5. Vertical structure of environment at 1200 UTC 20 Aug 2001. Skew *T* plots from (a) MID, (b) KCR, and (c) KJP. (d) The vertical *u*, *v* wind profile, and 200–850-hPa shear vector derived from the NCEP Global Tropospheric Analysis. For wind barbs, flag is 5 m s^{-1}, half-flag is 2.5 m s^{-1}, and pennant is 25 m s^{-1}.

Hurricane Bonnie's convective burst (Heymsfield et al. 2001). The environmental shear vector shows (Fig. 6, 2002 UTC panel) that cell 2 as well as other cells forming near the LLC are located downshear-to-downshear left of circulation center similar to what has been found in both the observational and modeling studies mentioned in the introduction.

The rapid growth of this burst is shown quantitatively in Fig. 7 with the minimum (cloud top) temperature of cells 1–3 (Fig. 7a), and anvil area expansion associated with cells 2 and 3 (Fig. 7b). The area curves were constructed from the sequence of ~15 min GOES IR images on 20 August by obtaining the number of pixels with IR brightness temperatures less than 194, 196, and 198 K centered on the convective burst. It was not possible to track higher temperature contours since they merged together from different cells. The cell 2 burst in Fig. 7 was by far the strongest during 20 August. Rapid growth of cell 2 to over 4000 km^2 is evident between about 2000 and 2130 UTC, and then its area declines from 2130 to 2230 UTC. The IR temperatures associated with this cell reach a minimum of ~193 K at about 2110 UTC, 20 min prior to the area maximum; a new cell (cell 3) begins development at ~2300 UTC.[1] The approximate stages of development of cell 2 are shown on the figure: the growth period, which occurs before and during the anvil expansion prior to the minimum temperature occurrence; mature convection during the anvil expansion and the minimum temperature occurrence; and dissipating stage during which the anvil area decreases and the cloud-top temperatures increase. Cell 3 was only observed during its more intense stage since it was obscured by cirrus in its early lifetime. Also indicated on the figure are times when the NASA aircraft crossed cell 2 during three flight legs; the DC-8 circumnavigated cell 2 during pass 2 because of prior icing conditions during pass 1. Passes 1 and 2 occurred during the active development of cell 2, and pass 3 occurred during the dissipation of the burst. The N42RF focused on this cell and later on cell 3, which was not studied by the NASA aircraft.

[1] The TRMM Visible and Infrared Scanner (VIRS) temperatures were lower than the GOES IR values probably because of the better VIRS resolution as compared with GOES (1-km pixel size vs 4 km) and the small dimensions of undiluted portions of individual cells.

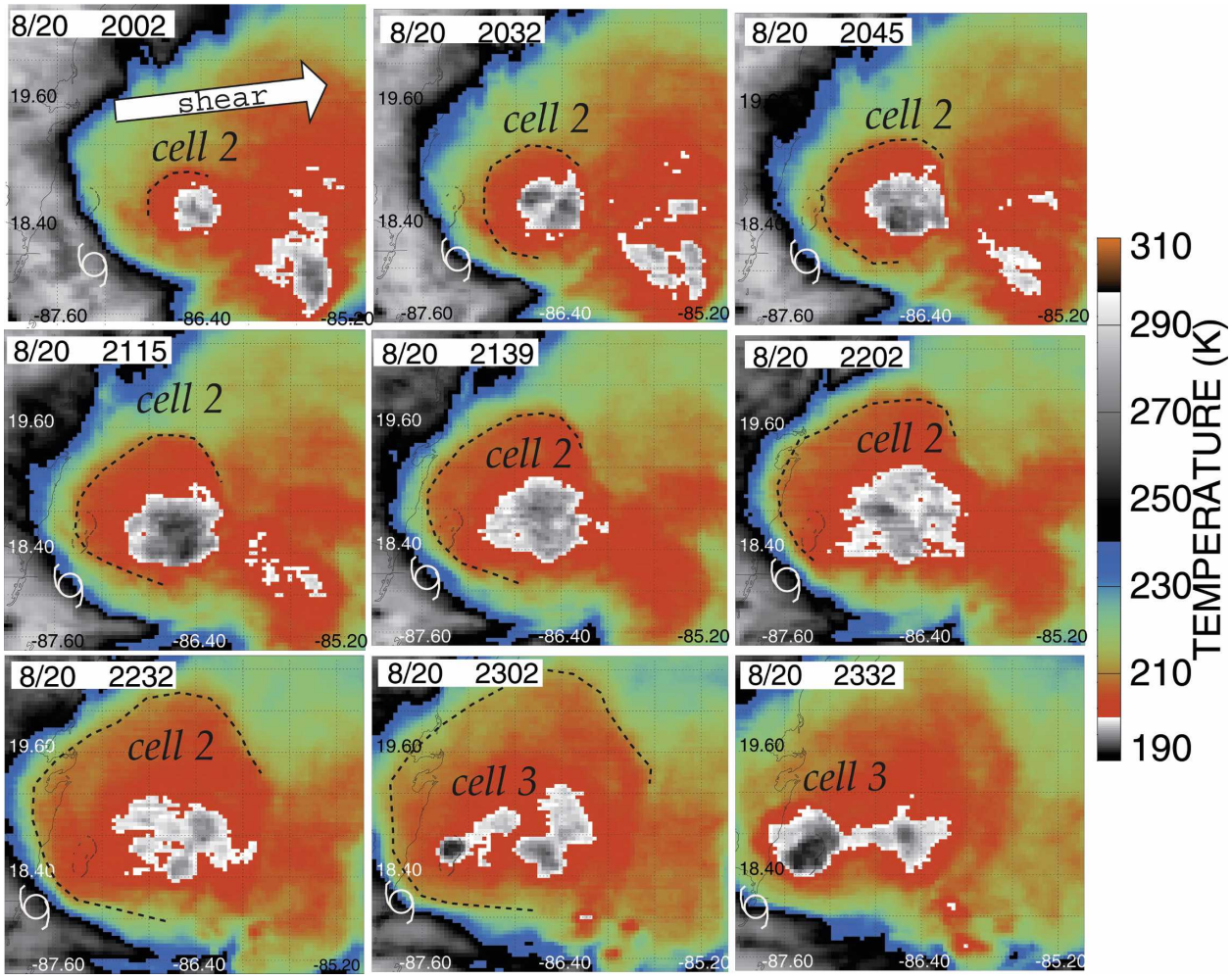

FIG. 6. The IR images covering the period of ER-2 flights on 20 Aug 2001. The color table highlights the cold overshooting cloud tops and the cirrus outflow from them. The two cells contributing toward the main convective burst and the expanding anvil are shown with dashed lines. The center obtained from the storm is indicated. The 2002 UTC panel shows the 200–850-hPa shear vector obtained from the NCEP 20 Aug 2001 at 1200 UTC analysis (Fig. 5d). Grid lines are in 0.4° intervals.

3. Mesoscale storm environment from dropsondes and flight-level data

a. Thermodynamic and wind analyses

The mesoscale environment of Chantal is examined here using a combination of dropsonde and DC-8 and N42RF flight level data. The DC-8 and P3 dropped 7 and 23 dropsondes, respectively, mostly near the circulation center and on the eastern side of the storm (Fig. 8); only a few of the dropsondes were located on the west side of the circulation. Details on the dropsondes are described in Hock and Franklin (1999). The N42RF flew at ~4.3 ± 0.1 km, whereas the DC-8 flew over a wider altitude range between ~10.5 and 12.6 km most of the time with a mean altitude ~11.7 km, but with one flight leg (pass 2) at ~9 km altitude. From these datasets, two-dimensional maps of various thermodynamic and winds were constructed at the mean aircraft altitudes of 11.7 and 4.3 km (Figs. 9a,b, respectively), and near the surface at 0.2 km (Fig. 9c) using only the dropsondes. The DC-8 flight level data used wind data from the Meteorological Measurement System (MMS; Chan et al. 1998) and moisture data from the JPL laser hygrometer (JLH; May 1998; Herman and Heymsfield 2003). Figures 9a,b provide storm-relative wind barbs (storm motion of 6 m s^{-1} toward 290°), θ_e contours, streamlines, and background images of GOES IR at 0215 UTC (Fig. 9a) and TMI 85 GHz (Figs. 9b,c respectively) at 2034 UTC. The LLC center was determined based on the wind measurements from the dropsondes and NOAA aircraft flight-level data that showed a well-defined circulation center. The locations

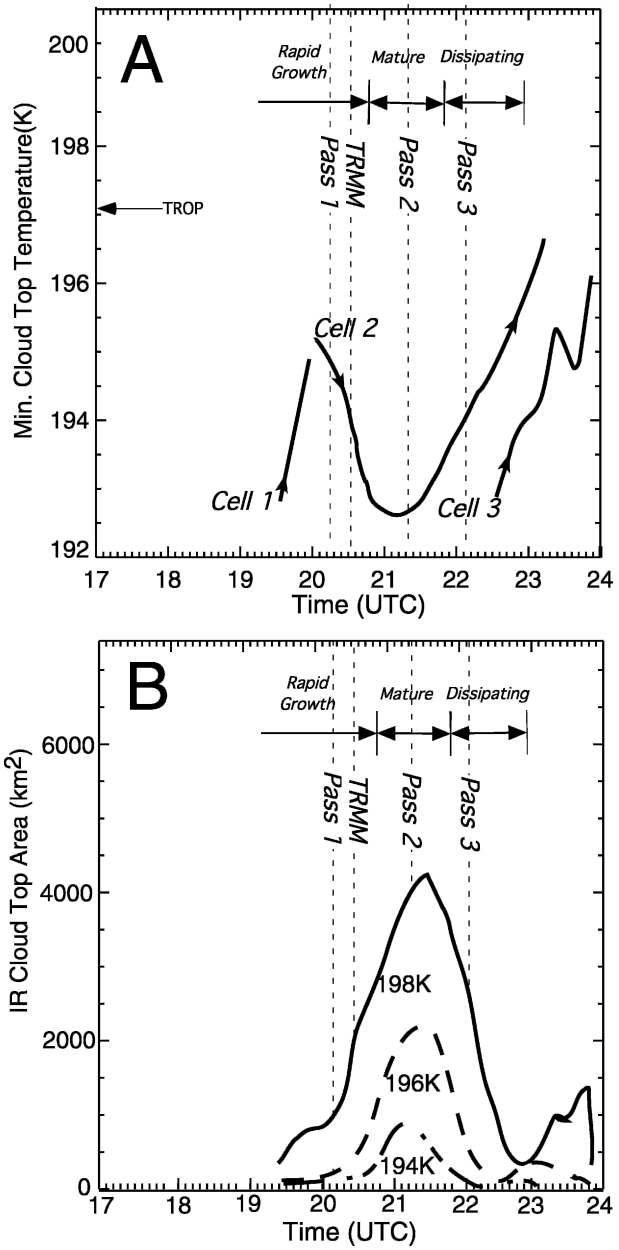

FIG. 7. Growth of cells in Chantal. Shown are cloud-top temperatures from (a) cells 1–3 and (b) IR cloud-top area. The area curves in (b) are thresholded for 194, 196, and 198 K. The times where the ER-2 passed across cell 2 (vertical dashed lines) provide a time reference. The tropopause minimum sounding temperature (~192 K) is indicated in (a). See text for details.

of both the aircraft flight-level and dropsonde data have been space–time adjusted to 2115 UTC since the datasets cover 3 h and the storm has moved ~65 km during this time. The storm-relative wind vectors were determined by subtracting the best-track storm motion (Fig. 2b). Narrowing the range of DC-8 altitudes has reduced the variation of θ_e from changes in the aircraft altitude. It is noted here that in some cases there may be an offset between the satellite and aircraft observations because of mapping errors in the satellite data arising from parallax or navigation errors. This can be on the order of 10–20 km for either satellite.

It is well known from WP-3D penetrations of hurricanes that θ_e measurements are prone to errors from sensor wetting (Eastin et al. 2002). In these events, the Rosemont 102 immersion deiced thermometer temperatures are significantly cooler than actual temperatures estimated from a Barnes radiometer in Eastin et al. The Barnes radiometer was unavailable during our flights, so a procedure suggested by R. Black (2004, personal communication) of NOAA Hurricane Research Division was used to remove questionable data. Temperatures from two fuselage-mounted sensors located a few feet apart were corrected for dynamic heating using the fuselage dynamic pressure sensor rather than those in the nose boom or wingtip. When wetting occurs, the temperature from that sensor will drop considerably. The two temperature measurements are used in combination and when one sensor's temperature drops by more than 1°C relative to the other sensor, then the higher temperature is used. It is rather obvious in Chantal when sensor wetting occurs although it is still possible that an error of a degree or two can occur. The DC-8 also had sensor wetting in a few occasions (Herman and Heymsfield 2003), although the occurrence is rare because of the DC-8's high altitude and the relative infrequency of supercooled water. Bolton's (1980) method was used to calculate θ_e. For both the WP-3D and DC-8, dewpoint temperatures that exceeded the air temperature were set to the air temperature in the calculation of θ_e. Eastin et al. (2002) mentioned that a measured supersaturated dewpoint temperature could actually result from a subsaturated region, causing a significant error in the dewpoint temperature. The resulting errors will not greatly affect following interpretations of the spatial and vertical structure of θ_e.

At 11.7-km DC-8 level (Fig. 9a), the large-scale southwest flow diverts around Chantal's convective region. Strong outflow divergence that is produced by cell 2 extends nearly 100 km upshear. The high θ_e (352 K) contour covers most of the convective region including its divergent outflow, and it extends significantly upshear over the LLC; a 354-K θ_e region exists upshear of the precipitation core of cell 2. The environmental θ_e at this altitude is ~350 K, so the higher observed θ_e at this altitude are in part due to convectively lifted air from low levels. Individual flight line traces show the θ_e maxima of ~355 K correspond to ~2 K higher air temperatures suggesting that the air is positively buoyant at

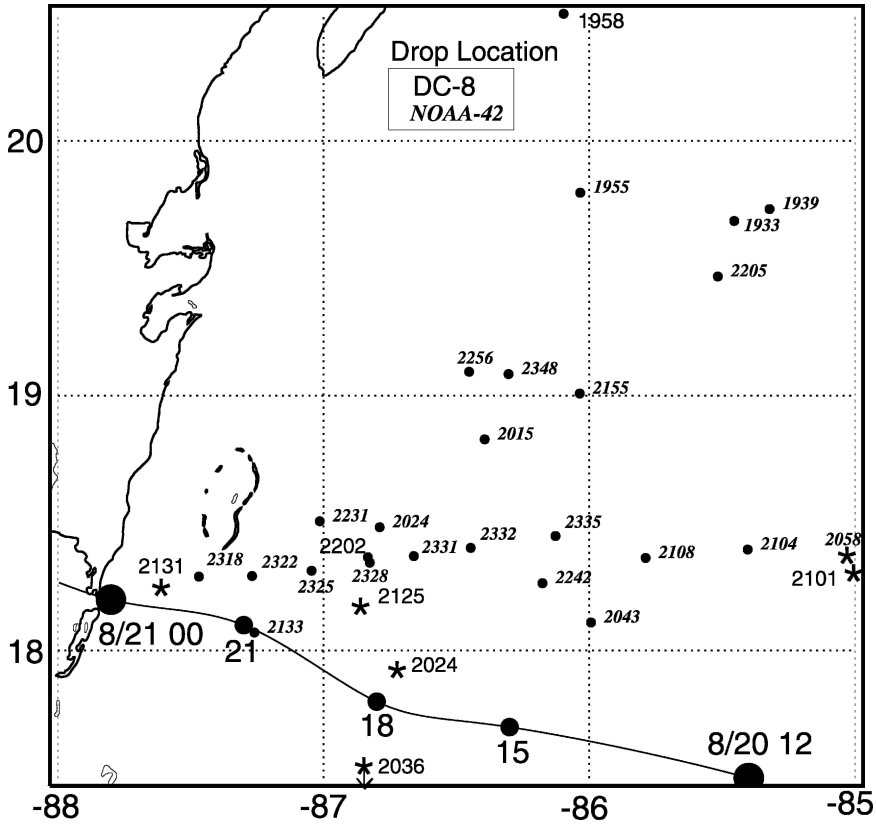

FIG. 8. Locations of dropsondes released from the DC = 8 and N42RF. The symbols used are storm best track (large and medium filled circles), dropsondes (small filled circle), and dropsondes used in Fig. 10 (★).

this ~12 km altitude. Away from the updraft core region in the anvil, the high θ_e region is due in part to subsidence that conserves θ_e. Analysis of the high convective available potential energy (CAPE) soundings indicates that the equilibrium level (EL) for a lifted parcel without mixing is about 15 km, suggesting that the higher temperatures in the updraft core region at 12-km altitude are likely positively buoyant. At 4.3-km altitude (Fig. 9b), a well-defined circulation center is observed that is tilted slightly northeast of the LLC position at 0.2 km. A northwest–southeast band of high 350–352-K θ_e (peak value 354–355 K) is located about 20–30 km southwest of the intense 85-GHz precipitation core of cell 2. This displacement between the high θ_e band and the core of cell 2 is due to subsidence warming that will be discussed further in section 4.

The LLC center is located ~80 km southwest of the main cell (cell 2 in Fig. 9c). High θ_e air (363 K) feeds the convection from the south side and converges spirally into an inflow notch northeast of the LLC. To the northeast of the convection, there is a broad pool of low θ_e values ~335 K. A large northwest–southeast θ_e gradient exists between the inflow sector and the outflow boundary along the southern side of cell 2. Strong easterly flow was present north of the LLC in the low θ_e downdraft region. The pressure distribution (not shown) shows that the lowest pressure (999 hPa) based on dropsondes was not associated with the LLC but rather with a mesolow across the main outflow boundary and θ_e ridge (350 K) northeast of the LLC ("L" in Fig. 9c). The surface flow is highly confluent into this mesolow with a 25 m s^{-1} easterly low-level jet (green contour) at the surface that is probably being accelerated into this mesolow. The inflow notch, not the LLC, has the greatest flow confluence, highest wind speeds, lowest surface pressure, and highest θ_e. This is all feeding the massive cell 2 hot tower that will be discussed further in section 4. The inflow notch region and cell 2 seems to be dynamically the most active region and not the LLC. There still may be lower pressures associated with the LLC, but the west side of the LLC was not sampled well by aircraft or dropsondes. This structure will be related later to the structure of Tropical Storm Isabel observed by SB92. Figure 10 shows profiles from dropsondes released by the DC-8 (2131, 2125, 2036, and 2101 UTC) at locations shown in Fig. 9c that capture

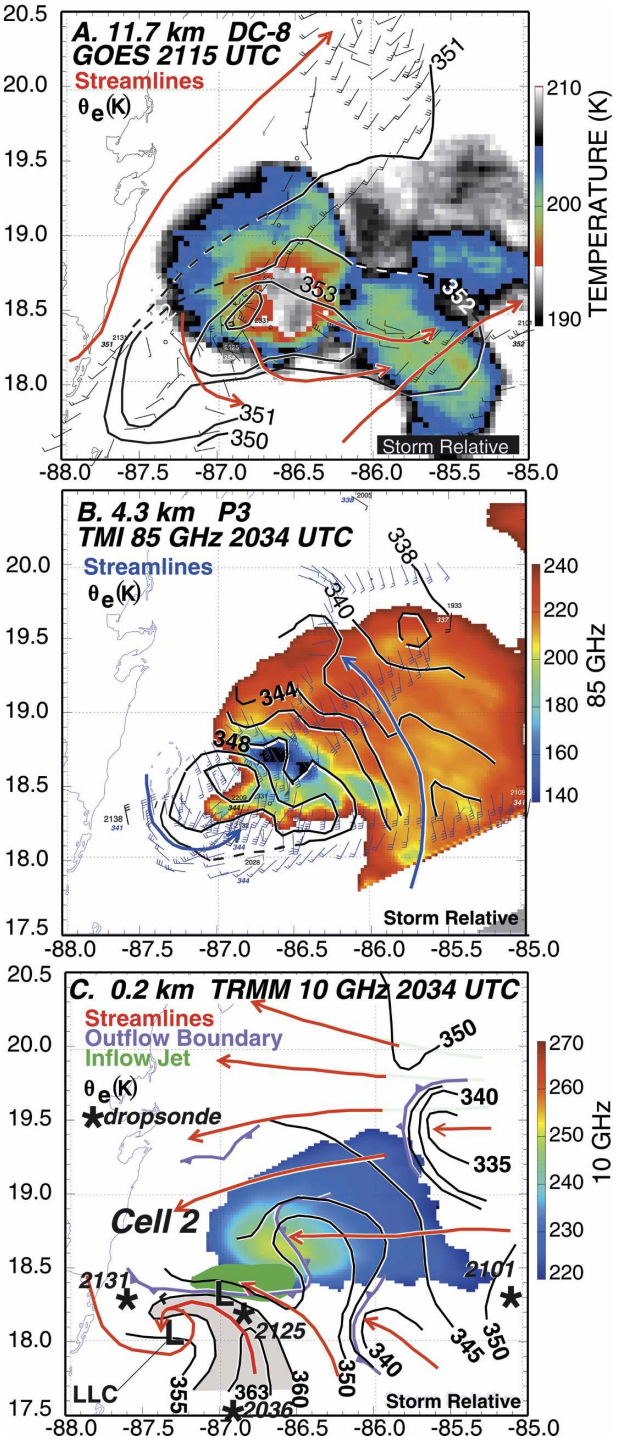

FIG. 9. Horizontal analyses based on flight-level data and dropsondes at (a) 11.7, (b) 4.3, and (c) 0.2 km MSL. The background images are from (a) GOES and (b), (c) TRMM satellite observations. All panels show θ_e contours at labeled values to highlight features (a) 1-K intervals from 350 to 354 K, (b) 2-K intervals from 338 to 350 K, and (c) 5-K intervals from 335 to 360 K with an additional 363-K contour; contours are dashed when extrapolated. Storm-relative wind barbs are given in (a) and (b) where pennant is 25 m s^{-1}, flag is 5 m s^{-1}, and half-flag is 2.5 m s^{-1}, and storm-relative streamlines are shown in all panels. See text for details.

key features of Chantal's structure. The θ_e ~335 K near the surface (Fig. 9c) likely originates from convective-scale downdrafts from the arc of high reflectivity north and east of the circulation center. The suggestion is that downdrafts with θ_e ~335 K originate from midlevels near the environment θ_e minimum at ~4 km altitude (Figs. 10a–c).

The CAPE was calculated for these soundings since it can provide insight on the storm dynamics and the DC-8 provided mid-upper tropospheric measurements that are often unavailable in developing storms. CAPE was estimated using an average parcel over the lowest 500 m that was lifted dry adiabatically up to the lifting condensation level (LCL), moist adiabatically up to the level of free convection (LFC), and moist adiabatically up to the equilibrium level. The CAPE was calculated from the positive area in sounding between the LFC and EL. For a few of the dropsondes with more than one EL, the upper (near tropopause) EL was chosen to avoid erroneously terminating the parcel at low levels due to an inversion. This low-level inversion is manifested as negative area or convective inhibition (CIN), and it is likely overcome by the strong frictional convergence and vertical motion associated with Chantal. Since data are required up the EL for the CAPE calculation and the DC-8 flight level is a few kilometers below the EL, missing sounding values were interpolated from the dropsonde latitude–longitude position in the 1800 UTC European Centre for Medium-Range Weather Forecasts (ECMWF) analysis; 5-s averages were performed on the soundings to reduce noise in the profiles. A few dropsondes were eliminated altogether since their top level was too low or humidity data was missing at low levels. Williams and Renno (1993) have reviewed three CAPE calculations for tropical atmospheres: irreversible or pseudoadiabatic, reversible, and reversible with ice processes. The calculated CAPE values above provides irreversible CAPE and not reversible CAPE, which gives lower values because it retains all the moisture in the parcel rather than letting it fall out; latent heating by fusion when supercooled water in convective updrafts is present was also not considered.

Table 1 shows the CAPE, the maximum CAPE below 700 hPa, the level of maximum CAPE, the LCL, and the LFC. The maximum CAPE differs from the CAPE for only one sounding (2202 UTC). The low CAPE soundings (1958 and 2202 UTC) have high LFC and also large CIN (not shown), the 2202 UTC sounding is clearly in downdraft air. The observed CAPE values associated more directly with the convection in Chantal (2036, 2125, 2131 UTC) are generally large compared with the core of a mature hurricanes where CAPE is ~400–800 J kg^{-1}, but they are less than what

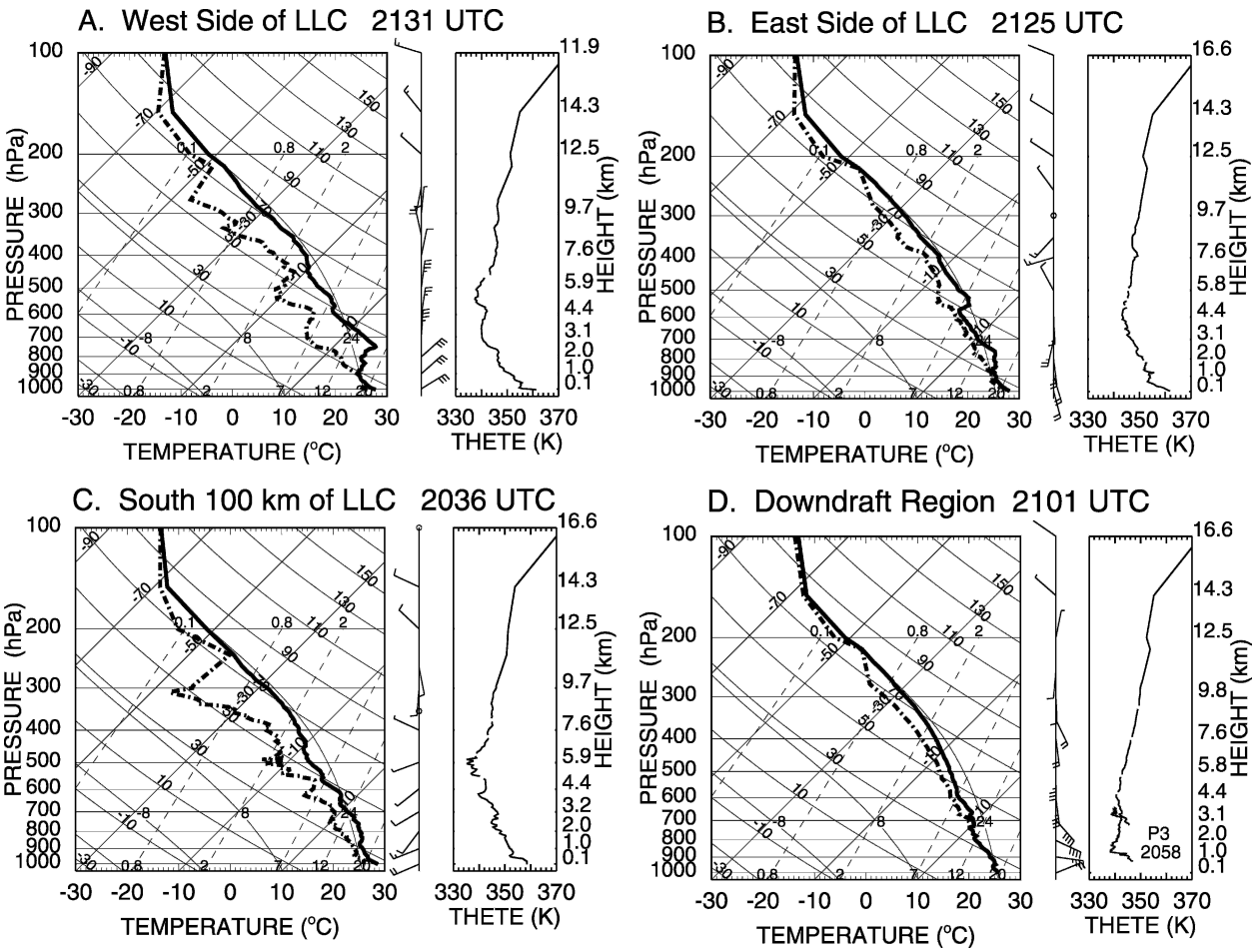

FIG. 10. Skew T and θ_e plots from dropsonde locations indicated by (★) in Fig. 8. Dropsondes are from the DC-8 except where (d) the 2101 UTC DC-8 θ_e is plotted along with the 2058 UTC P3 θ_e panel since there were no low-level dewpoint measurements from the DC-8 dropsondes. The 200-, 150-, and 100-hPa sounding values are interpolated from the 1800 UTC ECMWF analysis. For wind barbs, pennant is 25 m s^{-1}, flag is 5 m s^{-1}, and half-flag is 2.5 m s^{-1}.

would be encountered for an environment of extremely strong convection over the United States Bogner et al. (2000) found for six North Atlantic storms that CAPEs were large (1500–1700 J kg^{-1}) at large radii (>300 km), and they decreased from 1500 to ~200 J kg^{-1} by 75-km radius. Note that the upshear dropsonde in Chantal (2131 UTC; Fig. 10a) has 30%–45% lower CAPE than the two downshear drops (2036, 2125 UTC; Figs. 10c,b). This is consistent with there being subsidence and upper-tropospheric warming upshear. Only once the storm goes by and downshear upward motion occurs does the CAPE increase and convection breaks out. Various studies (e.g., Frank and Ritchie 1999) have shown that upward motion should be downshear left, which is where the convection is in Chantal. When CAPE is large, it is likely that convective updrafts are

TABLE 1. CAPE calculations from DC-8 dropsondes.

Time (UTC)	CAPE (J kg^{-1})	Max CAPE below 700 hPa (J kg^{-1})	Level of max CAPE (hPa)	LCL (hPa)	LFC (hPa)	Location
1958	327	327	Surface	916	754	Far north
2036	1523	1523	Surface	956	899	Downshear
2125	1555	1555	Surface	966	960	Downshear left
2131	1082	1082	Surface	969	955	Upshear
2202	538	1780	950	956	794	Downdraft

strong, larger hydrometeors are carried to mid- and higher levels, and strong downdrafts are over a deep layer because of water loading. For this situation, downdraft cooling near the surface may be offsetting surface fluxes and helping to prevent development of the storm. Raymond et al. (1998) and Bister and Emanuel (1997) argued that midlevel moistening was necessary before storms could intensify to hurricanes because it increases midlevel θ_e and thus minimizes cold downdrafts. The fairly large CAPE in Chantal may indicate that such a process has not yet occurred.

b. Warm core structure and midlevel subsidence

The data are examined here for the presence of a warm anomaly at lower and middle levels in the N42RF and DC-8 dropsonde data. How big is this anomaly, and where is it located with respect to both the MCS and the low-level vortex? Figs. 11a–d provide plots of the temperature perturbations (T') at the surface (50 m), 3-, 6-, and 8-km altitude over the same domain as in Fig. 9. The pressure perturbation (P') at the surface and 3-km levels is also shown in Figs. 11e,f. These perturbations were obtained by subtracting the temperature–height or pressure–height profile representative of the storm environment; profiles were constructed by averaging soundings and dropsondes that were farther out from Chantal's LLC (i.e., Fig. 5 and more distant DC-8 sondes). An attempt to incorporate the flight-level data into the temperature analysis was unsuccessful because of the varying height of the aircraft and the inability to correct the temperatures for these height changes. Since the dropsondes have incomplete coverage of the analysis domain, only a limited portion of the region is contoured.

The near surface level T' (SFC; Fig. 11a) depicts a weak warm region east-southeast of the LLC with a peak value of +1.3°C and slightly larger maximum of +1.9°C at the 2-km level (not shown). Two low pressure areas exist, one near the LLC (−5.7 hPa) and the other stronger area (−6.3 hPa) at the edge of cell 2. This latter mesolow is an inflow notch for cell 2 and the generally reflects the high θ_e air entering the MCS. An extensive area of low T' with a minimum of −2.5°C exists below cell 2, which is associated with the low θ_e downdraft air previously mentioned. At 3 km (Fig. 11b), there is significant warming over the LLC with a local maxima of $T' = +4.6$°C. This largely results from subsidence warming observed in the 2131 UTC sounding (Fig. 10a) that is also in the upshear right quadrant. The two low pressure areas still exist but with greatly reduced magnitude over the LLC ($-P' \sim 2.8$ hPa), and still a strong pressure minimum ($P' \sim -4.6$ hPa) immediately adjacent to cell 2 and at the head of its inflow. At 6 km (Fig. 11c), the warm core (maximum value +1.9°C) has shifted from the LLC, east-northeast along the shear vector. Part of this warming occurs along the upshear right periphery of cell 2 and partially within the cell itself. At 8-km altitude (Fig. 11d), an expanded warm region (T' maxima of ~1.5°C) occurs along the upshear and upshear right periphery of cell 2. And, by 10 km (not shown), there is no warm core outside of the cell 2 cloud region.

Summarizing the temperature structure, Chantal does not have one deep warm core typical of mature hurricane, but rather two areas of anomalous weak warming. One area is in the clear air directly above the LLC and seems most pronounced in the lower levels (<6 km altitude). The 2131 and 2125 UTC dropsondes (Figs. 10a,b) corroborate this warming and suggest intense subsidence (i.e., an inversion) in the 600–800-hPa layer. A second warm area above 5 km is more diffuse but is consistently located over the inflow notch (high θ_e inflow in Fig. 9c) in the vicinity of the most intense hot tower (cell 2), and has vertical continuity from about 4–5 to 8 km. The warming in the lower layers that is localized to the inflow notch/updraft area is likely due to enhanced surface heat fluxes and lack of convective downdrafts. This is supported by the previous CAPE values in Table 1. The warming in the upper layers is more spread out and on the edge of the MCS, and there are several possible mechanisms for this broad area of midlevel warming: 1) from compensating midlevel subsidence induced by cell 2, and 2) the easterly outflow aloft colliding with the upper-level environmental westerlies causing subsidence warming (e.g., Ritchie and Elsberry 2001). Simpson et al. (1997) in their study of Tropical Storm Oliver also found development of a circulation center and eye adjacent to a major MCS and argued that subsidence in the adjacent regions helped contribute to the storms development. They found convection-related warm cores (the main more compact core 3–5 K at low levels and tilted into the convective region, and the other linked to a second MCS) that corroborate a link between the convection and the subsidence. They argued that subsidence is the only process that can maintain the low-level warm anomaly in clear air, whereas subsidence and latent heating appear to contribute to midlevel warming.

There are also interesting similarities between the Tropical Storm Chantal observations and the SB92 study of Tropical Storm Isabel. Even though there was no obvious jump in Chantal's track as was observed for Isabel, it is clearly possible that Chantal's LLC is a second vortex development after dissipation of a primary vortex associated with cell 2. The LLC may have been swept out by the strong outflow boundary associ-

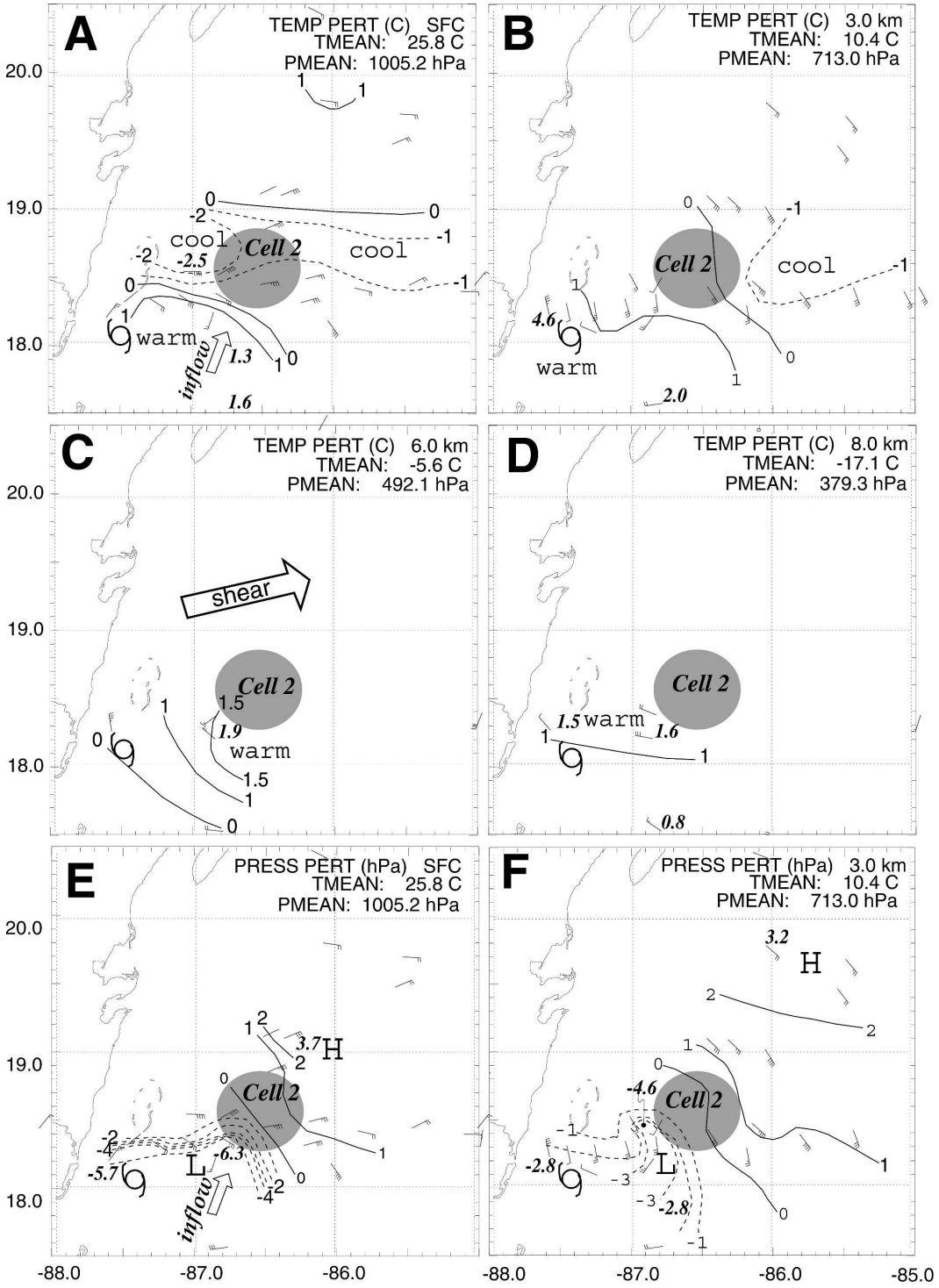

FIG. 11. (a)–(d) Horizontal analyses of temperature perturbation at 50 m (SFC), 4-, 6-, and 8-km altitude and (e), (f) pressure perturbation at SFC and 4-km altitude based on dropsonde data. The approximate location of cell 2 (gray-shaded circular region), the LLC, and low (L) and high (H) pressure centers are indicated on each panel. Contours are given in 1°C and 1-hPa intervals except where noted; negative contours are dashed. Local minima and maxima are shown in italics.

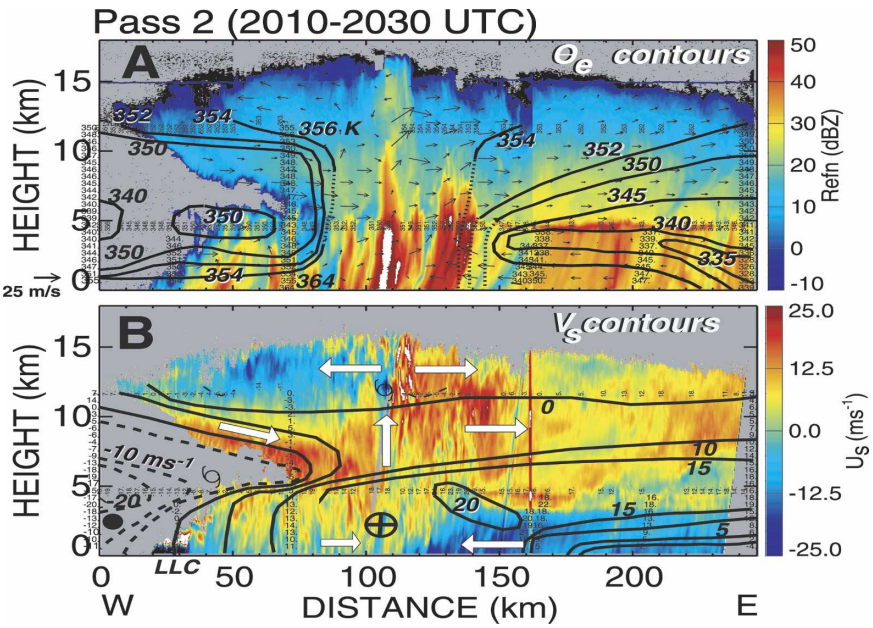

FIG. 12. Cross section obtained from EDOP for pass 2 between 2101 and 2125 UTC. (a) A color-enhanced reflectivity image with superimposed storm relative wind vectors obtained from EDOP, with contours of θ_e (black); θ_e contours are dotted in data-sparse convective region. (b) A color-enhanced image of storm-relative along-track winds (U_s) with superimposed contours of the storm-relative across-track (V_s) wind component (black). Large white vectors provide general sense of along-track flow. The contours are based on the DC-8 and P3 flight-level and dropsonde data; they are dashed in the convective region where data are too sparse to draw contours. Positive V_s is into the page and the vortex maximum winds are noted by solid dot (into page) and + (out of page). The orientation of the section is shown in Fig. 3. Reflectivities (w) exceeding 50 dBZ (8 m s^{-1}) are white, and w less than -8 m s^{-1} are black. Locations of dropsonde start times are in italics; dropsonde and flight-level data are indicated with small numbers. The red column at distance 160 km is due to the ER-2 making a 360° turn to allow time for the DC-8 to catch up with it. The DC-8 and N42RF flight-level circulation centers are indicated by circulation symbol.

ated with cell 2, although there is insufficient data on the evolution of the LLC to determine this. In Chantal, both the LLC and cell 2 have an associated pressure minimum with a pressure perturbation of ~6 hPa at the surface; Isabel had approximately a 2-hPa perturbation. SB92 estimated that a 2–3-hPa pressure perturbation could be hydrostatically induced below a warm (2–3 K warmer than environment), dry layer 3–4 km thick similar to that observed in Isabel. The subsidence layer in Chantal is comparable to that observed by SB92, so it is quite plausible that the LLC may have been formed by a similar process. Further discussion on this will be given in the next section.

4. Convection and sustenance mechanisms

The convective region in Chantal was vigorous and long-lived and one key question is what maintains this convection and how does it interact with the shallow vortex described in the previous section. Another key question is whether the low-level observed warming adjacent to cell 2 and upshear right of the LLC is due to convective-induced subsidence or shear-induced subsidence (Frank and Ritchie 2001). The EDOP data from ER-2 passes across the convection and LLC provide some insights on the above questions. The main three ER-2 and DC-8 passes across Chantal covered ~2010–2030 UTC (pass 1), ~2101–2125 UTC (pass 2), and ~2148–2224 UTC (pass 3) as shown in Fig. 3b. EDOP was not turned on until near the end of pass 1, so cross sections from passes 2 and 3 are presented in the following. Figure 12 (Fig. 13) shows the EDOP-derived cross section for pass 2 (pass 3). The analysis procedures for the EDOP data are discussed in Heymsfield et al. (1999, 2001) and the procedures here are similar. The reflectivity image is shown in Figs. 12a and 13a along with storm-relative wind vectors in the cross section and contours of θ_e. Figures 12b and 13b show an

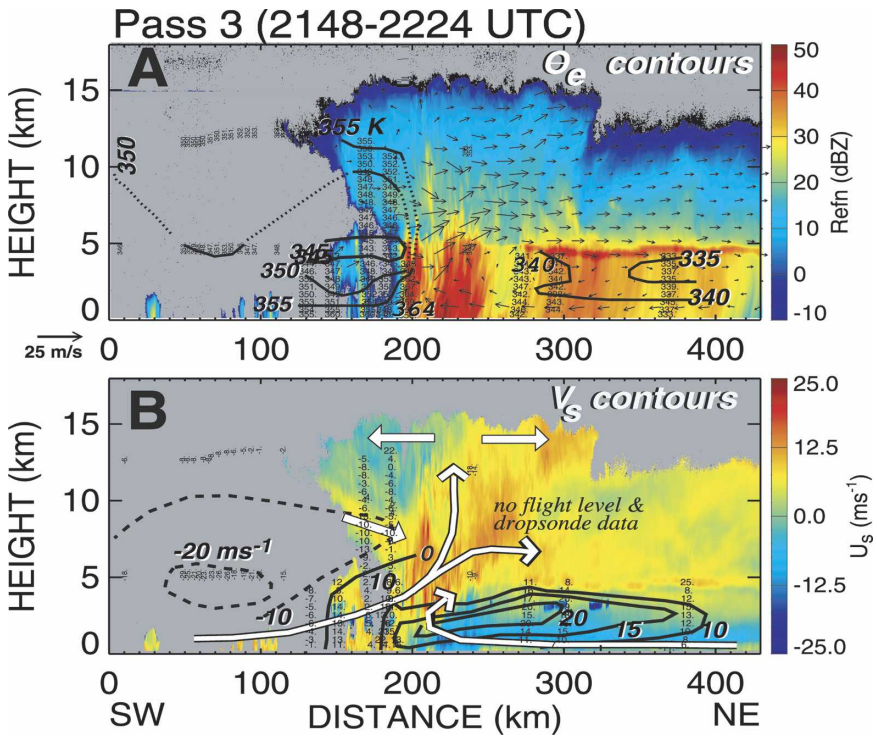

FIG. 13. Similar to Fig. 12, except for pass 3 at 2148–2224 UTC.

image of the along-track storm-relative wind component (U_s) derived from EDOP dual-beam data, superimposed contours of storm-relative tangential wind (V_s), and streamlines of airflow. The vertical profiles in the reflectivity images are attenuation corrected using the surface reference approach, and vertical air motions in the wind vectors are estimated from the Doppler velocities using hydrometeor fall speeds based on empirical relations in Heymsfield et al. (1999, 2001). The largest uncertainties occur in convective regions where there is mixed phase occurring above the freezing level. The wind vectors in the plane of the cross section have been obtained from EDOP's dual beams, and are presented as storm-relative assuming a storm motion 6 m s^{-1} toward 290°. The θ_e values in Figs. 12 and 13 were derived from both the DC-8 and N42RF dropsonde and flight-level data mapped to the cross section; these did not cover the entire cross section so some of the contours terminate or have arrows to denote this.

a. Pass 2: Along-shear vertical structure (Fig. 12)

There are several prominent features evident in this section that is approximately along the shear vector. 1) The LLC depicted by the V_s contours in Fig. 12b is located at a distance of ~30 km. 2) The major cell 2 in pass 2 in Fig. 12a (distance scale ~110 km) is extremely intense with peak reflectivities exceeding 55 dBZ, cloud top extending up to 17-km altitude, which is well above the tropopause. The earlier DC-8 flight through this convection (pass 1) recorded 22 m s^{-1} peak updrafts, ~10-km-wide region of updrafts greater than 5 m s^{-1}, and peak θ_e of 355–356 K in the convection core. The DC-8 flight-level data during pass 2 did not go through cell 2's core, but still recorded 8 m s^{-1} updrafts and θ_e of ~356 K; the environment θ_e was ~350 K. 3) This strong cell produces larger upper-level diffluence above 11-km altitude, and the high θ_e air carried aloft from low levels diverges over 200 km from the updraft core, producing a high θ_e core above the convection and not above the LLC. 4) A large region of low θ_e ~330–340 K is located to the east of the strong convection below a pronounced bright band. This region is likely the result of earlier downdrafts produced by convection as mentioned earlier. Also, the low-level easterlies particularly below 1-km altitude are faster than Chantal's movement, pass through this low θ_e region, and confluence results along the leading edge of this flow and the inflow jet feeding cell 2. This inflow jet of high-speed, high θ_e air feeding cell 2 is located at a distance of 110 km, at low levels in Fig. 12b. 5) Upper-level (5–10-km altitude) westerly flow subsides on the west side of cell 2 above the LLC, and undercuts the upper-tropospheric outflow from the cell. The interaction of the

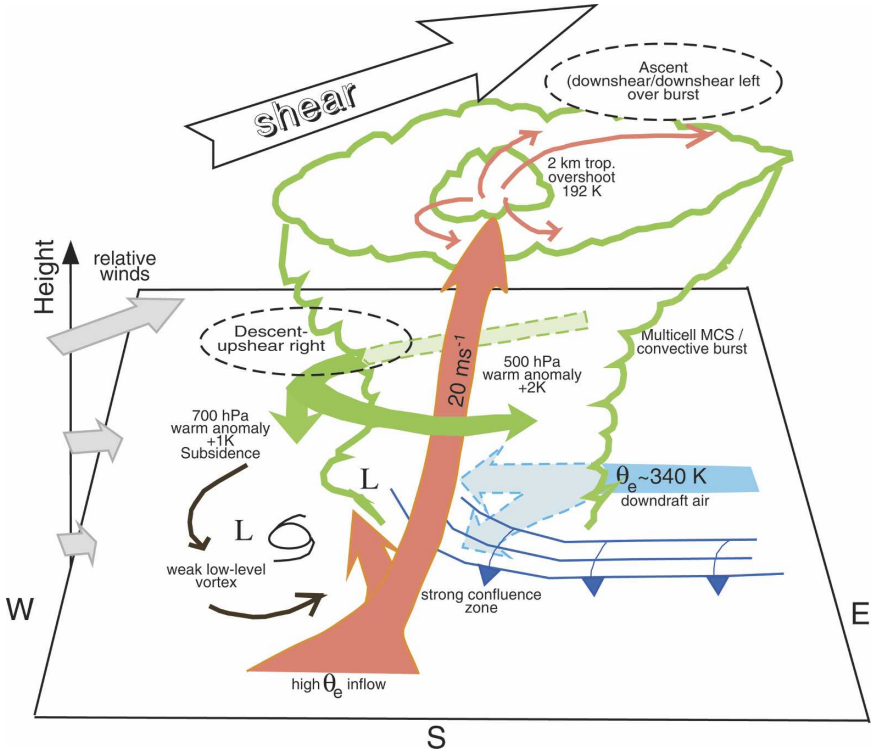

FIG. 14. Conceptual summary of Tropical Storm Chantal derived from aircraft and satellite observations.

westerly shear with this strongly divergent outflow likely results in a broad region of subsidence warming near the cell (Figs. 11c,d). 6) The vortex center tilt based on the flight-level data at the DC-8 and N42RF altitudes is highly sheared to the east as depicted by the flight-level circulation centers.

b. Pass 3: Convection tilt (Fig. 13)

Pass 3 is located east of the LLC, running southwest to northeast (Fig. 3b), and it emphasizes the tilt of cell 2 as it was weakening. There was less data available from dropsondes and flight-level data for this pass, so not all of the contours are continued into the data-sparse regions. There are several additional features to note from this pass. 1) The updraft has a strong north-northeast tilt over low-level, low θ_e, easterly flow, and it has a top of about 16 km. 2) There is strong horizontal shear between the high θ_e air to the south (i.e., inflow) and the low θ_e downdraft produced air in the heavy rain region to the north-northeast. The downdraft air is located below about 4-km altitude and has θ_e values characteristic of ~4 km environmental values. 3) The DC-8 measured an updraft ~8 m s^{-1} at 2205 UTC (distance ~230 km in Fig. 13) with a spike of θ_e ~358 K, but with more typical 354-K values in the updraft core. Again, this high θ_e could only originate from the inflow sector air, south of the convection. 4) High θ_e air (353–355 K) again exists in the upper-level divergent outflow region near 12-km altitude. The DC-8 in situ winds are strongly divergent at 12-km altitude near the cell 2 core (Fig. 9a). 5) There are midlevel downdrafts along the southwest flank of the cell (distance ~160–190 km and altitude 8–10 km), which are related to the gentle subsidence mentioned in section 4a.

5. Summary and conclusions

The Tropical Storm Chantal study presented here has provided one of the first observational studies examining a weak tropical storm that struggled to intensify in a highly sheared environment with most of the shear above 700 hPa. Figure 14 summarizes Chantal's three-dimensional structure as deduced from the observations. The unusual aspect of Chantal was that it had a poorly defined vortex that only extended up to midlevels, and an adjacent intense convective region that comprised an MCS. The only low-level circulation (LLC) observed was in the rain-free region about 80 km to the west-southwest of the MCS, suggesting that it was possibly a new circulation center forming away from one originally associated with the MCS. This LLC

may have developed in a manner similar to the secondary circulation formation suggested by SB92 for Tropical Storm Isabel. The MCS appears to have been primarily the result of intense convergence between large-scale, low-level easterly flow and the cyclonic vortex flow. The individual cells in the MCS, such as cell 2 during the period of the observations, were extremely intense with core diameters of 10 km and peak updrafts exceeding 20 m s^{-1}. The easterly flow supporting the low-level convergence was highly modified by downdrafts from prior convection resulting in a strong θ_e and thermal boundary with the high θ_e air feeding the strongest cell 2 and low θ_e downdraft air to the northeast of this boundary. Interestingly, this strong low-level thermal boundary is favorable for vertical vorticity generation as the baroclinically across the gradient may be tilted into the vertical. But there did not appear to be intensification of a circulation in this region even though a local mesolow was present.

Associated with Chantal's MCS were two broad subsidence (warm) regions both of which had portions over the LLC. The first layer near 700 hPa was directly above the vortex and covered most of it. The second layer near 500 hPa was along the south and southwest flanks of cell 2 and undercut the anvil divergence region above. There was not much resemblance of these subsidence layers to typical warm cores in mature hurricanes. There are, however, similarities between Chantal's subsidence regions and those observed for Tropical Storm Oliver (Simpson et al. 1997). They attributed their observed warming to moist processes in the upper troposphere, and a combination of latent heating and adiabatic subsidence in the lower and midtroposphere. There is also strong resemblance of Chantal's subsidence regions to the SB92 Isabel observations where it was suggested that a deep subsidence layer may produce lowering of the surface pressure through midlevel warming below an anvil region associated with earlier convection. The mechanism for vortex generation and intensification is consistent with what has been suggested by Simpson et al., but it is somewhat different than has been suggested by Raymond and Jiang (1990), Bister and Emanuel (1997), and others that argue more toward a top-down mechanism where the initial MCV develops in midlevels in association with MCS stratiform regions, and the vortex develops downward.

The observed structure of Chantal relates in a general sense to theoretical and modeling studies of a vortex in a sheared environment. The convection in Chantal forms downshear left, and the free-atmosphere subsidence in the clear air at low levels with associated warming was found to be upshear as expected from the Ritchie and Elsberry (2001) moist simulation. The observed large vertical shear toward the northeast in Chantal resulted in a strong upper-level relative flow toward the northeast, and it may have had a significant effect on the storm intensification. Most of the warm, high θ_e, detrained midlevel air from the MCS and particularly cell 2, was carried off to the northeast by the strong relative flow, rather than being advected over the LLC; most of the observed subsidence warming over the LLC appears to be compensatively driven in response to the large upward mass fluxes in the MCS. Interestingly, the warming observed at upper levels in the outflow region of cell 2 was probably due to latent heating in the strong updrafts not being compensated by adiabatic cooling. From modeling studies, Frank and Ritchie (2001) found that strong shear produces asymmetries in the upper troposphere such that high values of θ_e and potential vorticity are mixed outward rather than into the eye. They speculated that shear ventilates the eye resulting in a loss of the warm core at upper levels that will raise the storm's central pressure and weaken the storm. A recent study by Emanuel et al. (2004) used a simple coupled ocean–atmosphere model to examine the influence of various environmental factors on tropical cyclone intensity using Tropical Storm Chantal as one of the cases. They found that shear and midlevel moistening had a major effect on Chantal's intensity. In their model, shear affects the model mainly through ventilation of the core with environmental midlevel air.

As mentioned earlier, the LLC in Tropical Storm Chantal may have been a secondary vortex that developed in a rain-free region away from the large MCS with intense convection. Even though there was midlevel subsidence above the vortex that was favorable for lowering its central pressure hydrostatically, it failed to intensify similar to what SB92 found for Tropical Storm Isabel. Unfortunately, the observations were not suitable for studying a longer period of the evolution of this LLC. However, Chantal may be examined in a very general sense in terms of WISHE theory (Emanuel 1986). Two of the WISHE assumptions are not met for Chantal that may have prevented it from intensifying: the presence of an asymmetric vortex and lack of a slantwise neutral sounding in the vortex region. The large CAPE values associated with this vortex clearly argue against slantwise neutrality. The lack of midlevel moisture over the LLC in Chantal is also unfavorable for the WISHE mechanism to be operative. It is likely that the tropospheric shear is simply too strong and that weaker shear would have resulted in more favorable interactions between the vortex and the strong convective towers. Instead, the convection (particularly cell 2) was so strong that the drier subsidence

layer over the LLC may have been compensatory flow. The Hurricane Bonnie (Heymsfield et al. 2001) study showed how strong hot towers may have a positive influence on storm intensification, that is, detrained high θ_e from the towers was found to be subsiding and contributing toward intensifying the storm's warm core. This was clearly not present in Chantal.

The original objectives for the Chantal mission were not to study the role of shear on the storm but rather the structure of the convection. As a result, there were barely enough dropsondes on the west side of the LLC for this study, and only one flight was performed for this storm. Also, dropsondes could not be released over land during a period when Chantal was approaching Belize. It is clear that shear and other many atmosphere and ocean properties are key in understanding why some storms intensify and others do not. These require a combination of focused observational studies that will provide more complete information of the storm details, and a broader set of assumptions in the modeling that incorporates more of the observational results.

Acknowledgments. The primary author's work was supported under the NASA CAMEX-4 research announcement sponsored by NASA Headquarters program manager Dr. Ramesh Kakar. We are especially appreciative of Dr. Frank Marks, Mr. Michael Black, and Dr. Robert Black of the Hurricane Research Division of NOAA who were a critical part of obtaining the datasets from Chantal and for providing basic information and mission summaries. We have had scientific discussions with Dr. John Gamache and others at HRD, and Dr. Scott Braun at Goddard. On the NASA side, Ms. Robbie Hood and Dr. Ed Zipser were key in directing the mission on this day, and many others provided key roles in the Chantal flights. Numerous data sources were used for this paper for which we are grateful. A number of the datasets were obtained from the CAMEX-4 archive at the Global Hydrology Resource Center sponsored by NASA's Atmospheric and Remote Sensing Program. Mr. Paul Bui of Ames Research Center (MMS instrument) and Dr. Robert Herman of JPL (JLH instrument) are especially acknowledged for providing DC-8 flight-level winds and moisture, respectively. Mr. David Vollaro is appreciated for performing the CAPE calculations used in the paper. Finally, one of the reviewers was particularly helpful in his thorough review of the manuscript.

REFERENCES

Bender, M. A., 1997: The effect of relative flow on the asymmetric structure of the interior of hurricanes. *J. Atmos. Sci.,* **54,** 703–724.

Bister, M., and K. Emanuel, 1997: The genesis of Hurricane Guillermo: TEXMEX analyses and a modeling study. *Mon. Wea. Rev.,* **125,** 2662–2682.

Black, M. L., J. Gamache, P. Dodge, G. Barnes, F. Marks, J. Hudson, and T. Castells, 2001: Mission summary: Tropical Storm Chantal. NOAA/Hurricane Research Division, 23 pp. [Available from NOAA/AOML/Hurricane Research Division, 4301 Rickenbacher Drive, Miami, FL 33149-1026.]

——, J. F. Gamache, F. D. Marks Jr., C. R. Samsury, and H. Willoughby, 2002: Eastern Pacific Hurricanes Jimena of 1991 and Olivia of 1994: The effect of vertical shear on structure and intensity. *Mon. Wea. Rev.,* **130,** 2291–2312.

Bogner, P. B., G. M. Barnes, and J. L. Franklin, 2000: Conditional instability and shear for six hurricanes over the Atlantic Ocean. *Wea. Forecasting,* **15,** 192–207.

Bolton, D., 1980: The computation of equivalent potential temperature. *Mon. Wea. Rev.,* **108,** 1046–1053.

Chan, K. R., J. Dean-Day, S. W. Bowen, and T. P. Bui, 1998: Turbulence measurements by the DC-8 meteorological measurement system. *Geophys. Res. Lett.,* **25,** 1355–1358.

Corbosiero, K. L., and J. Molinari, 2002: The effects of vertical wind shear on the distribution of convection in tropical cyclones. *Mon. Wea. Rev.,* **130,** 2110–2123.

DeMaria, M., 1996: The effect of vertical shear on tropical cyclone intensity change. *J. Atmos. Sci.,* **53,** 2076–2087.

Eastin, M. D., P. G. Black, and W. M. Gray, 2002: Flight-level thermodynamic instrument wetting errors in hurricanes. Part I: Observations. *Mon. Wea. Rev.,* **130,** 825–841.

Emanuel, K. A., 1986: An air–sea interaction theory for tropical cyclones. Part I: Steady-state maintenance. *J. Atmos. Sci.,* **43,** 585–604.

——, C. DesAutels, C. Holloway, and R. Korty, 2004: Environment control of tropical storm intensity. *J. Atmos. Sci.,* **61,** 843–858.

Frank, W. M., and E. A. Ritchie, 2001: Effects of vertical wind shear on the intensity and structure of numerically simulated hurricanes. *Mon. Wea. Rev.,* **129,** 2249–2269.

——, and ——, 1999: Effects of environmental flow upon tropical cyclone structure. *Mon. Wea. Rev.,* **127,** 2044–2061.

Franklin, J. L., S. J. Lord, S. E. Feuer, and F. D. Marks Jr., 1993: The kinematic structure of Hurricane Gloria (1985) determined by nested analyses of dropwindsonde and Doppler radar data. *Mon. Wea. Rev.,* **121,** 2433–2451.

Gallina, G. M., and C. S. Velden, 2000: A quantitative look at the relationship between environmental vertical wind shear and tropical cyclone intensity change utilizing enhanced satellite derived wind information. Preprints, *24th Conf. on Hurricanes and Tropical Meteorology,* Ft. Lauderdale, FL, Amer. Meteor. Soc., 256–257.

Gentry, R. C., T. T. Fujita, and R. C. Sheets, 1970: Aircraft, spacecraft, satellite and radar observations of Hurricane Gladys, 1968. *J. Appl. Meteor.,* **9,** 837–850.

Gray, W., 1968: Global view of the origin of tropical disturbances and tropical storms. *Mon. Wea. Rev.,* **96,** 669–700.

Herman, R. L., and A. J. Heymsfield, 2003: Aircraft icing at low temperatures in Tropical Storm Chantal (2001). *Geophys. Res. Lett.,* **30,** 1955, doi:10.1029/2003GL017746.

Heymsfield, G. M., and Coauthors, 1996: The EDOP radar system on the high altitude NASA ER-2 aircraft. *J. Atmos. Oceanic Technol.,* **13,** 795–809.

——, J. B. Halverson, and I. J. Caylor, 1999: A wintertime gulf coast squall line observed by EDOP airborne Doppler radar. *Mon. Wea. Rev.,* **127,** 2928–2949.

——, ——, J. Simpson, L. Tian, and P. Bui, 2001: ER-2 Doppler radar (EDOP) investigations of the eyewall of Hurricane Bonnie during CAMEX-3. *J. Appl. Meteor.,* **40,** 1310–1330.

HFP, 2001: Hurricane field program plan. Hurricane Research Division. [Available from Hurricane Research Division, NOAA/Atlantic Oceanographic and Meteorological Laboratory, 4301 Rickenbacher Drive, Miami, FL 33149-1026.]

Hock, T. F., and J. L. Franklin, 1999: The NCAR GPS dropwindsonde. *Bull. Amer. Meteor. Soc.,* **80,** 407–420.

Holliday, C. R., and A. H. Thompson, 1979: Climatological characteristics of rapidly intensifying typhoons. *Mon. Wea. Rev.,* **107,** 1022–1034.

Hood, R. E., and Coauthors, 2006: Classification of tropical oceanic precipitation using high-altitude aircraft microwave and electric field measurements. *J. Atmos. Sci.,* **63,** 218–233.

Jones, S. C., 1995: The evolution of vortices in vertical shear. Part I: Initially barotropic vortices. *Quart. J. Roy. Meteor. Soc.,* **121,** 821–851.

Malkus, J. S., and H. Riehl, 1960: On the dynamics and energy transformations in steady state hurricanes. *Tellus,* **12,** 1–20.

Marks, F. D., Jr., R. A. Houze Jr., and J. F. Gamache, 1992: Dual-aircraft investigation of the inner core of Hurricane Norbert. Part I: Kinematic structure. *J. Atmos. Sci.,* **49,** 919–942.

May, R. D., 1998: Open-path, near-infrared tunable diode laser spectrometer for atmospheric measurements of H_2O. *J. Geophys. Res.,* **103,** 19 161–19 172.

Molinari, J., D. Vollaro, and K. L. Corbosiero, 2004: Tropical cyclone formation in a sheared environment: A case study. *J. Atmos. Sci.,* **61,** 2493–2509.

——, P. Dodge, D. Vollaro, K. L. Corbosiero, and F. Marks, 2006: Mesoscale aspects of the downshear reformation of a tropical cyclone. *J. Atmos. Sci.,* **63,** 341–354.

Montgomery, M. T., and J. Enagonio, 1998: Tropical cyclogenesis via convectively forced vortex Rossby waves in a three-dimensional quasi-geostrophic model. *J. Atmos. Sci.,* **55,** 3176–3207.

QuikSCAT, 2001: QuikSCAT science data product user's manual: Overview and geophysical data products. Version 2.2, Jet Propulsion Laboratory D-18053, 89 pp.

Raymond, D. L., and H. Jiang, 1990: A theory for long-lived mesoscale convective systems. *J. Atmos. Sci.,* **47,** 3067–3077.

——, C. Lopez-Carrillo, and L. Lopez Cavazos, 1998: Case-studies of developing east Pacific easterly waves. *Quart. J. Roy. Meteor. Soc.,* **124,** 2005–2034.

Ritchie, E. A., and G. J. Holland, 1997: Scale interactions during the formation of Typhoon Irving. *Mon. Wea. Rev.,* **125,** 1377–1396.

——, and R. L. Elsberry, 2001: Simulations of the transformation stage of the extratropical transition of tropical cyclones. *Mon. Wea. Rev.,* **129,** 1462–1480.

——, J. Simpson, W. T. Liu, J. Halverson, C. S. Veldon, K. F. Brueske, and H. Pierce, 2003: Present day satellite technology for hurricane research. *Hurricane! Coping with Disaster*, R. H. Simpson, Ed., Amer. Geophys. Union, 249–289.

Rogers, R., S.-C. Chen, J. Tenerelli, and H. Willoughby, 2003: A numerical study of the impact of vertical shear on the distribution of rainfall in Hurricane Bonnie (1998). *Mon. Wea. Rev.,* **131,** 1577–1599.

Sadowy, G. A., A. C. Berkun, W. Chun, E. Im, and S. L. Durden, 2003: Development of an advanced airborne precipitation radar. *Microwave J.,* **46,** 84–98.

Simpson, J., E. Ritchie, G. J. Holland, J. Halverson, and S. Stewart, 1997: Mesoscale interactions in tropical cyclone genesis. *Mon. Wea. Rev.,* **125,** 2643–2661.

——, J. B. Halverson, B. S. Ferrier, W. A. Petersen, R. H. Simpson, R. Blakeslee, and S. L. Durden, 1998: On the role of "hot towers" in tropical cyclone formation. *Meteor. Atmos. Phys.,* **67,** 15–35.

Steranka, J., E. B. Rodgers, and R. C. Gentry, 1986: The relationship between satellite measured convective bursts and tropical cyclone intensification. *Mon. Wea. Rev.,* **114,** 1539–1546.

Stossmeister, G. J., and G. M. Barnes, 1992: The development of a second circulation center within Tropical Storm Isabel (1985). *Mon. Wea. Rev.,* **120,** 685–697.

Trier, S. B., C. A. Davis, and W. C. Skamarock, 2000: Long-lived mesoconvective vortices and their environment. Part II: Induced thermodynamic destabilization in idealized simulations. *Mon. Wea. Rev.,* **128,** 3396–3412.

Wentz, F. J., C. Gentemann, D. Smith, and D. Chelton, 2000: Satellite measurements of sea surface temperature through clouds. *Science,* **288,** 847–850.

Williams, E., and N. Renno, 1993: An analysis of the conditional instability of the tropical atmosphere. *Mon. Wea. Rev.,* **121,** 21–36.

Zehr, R. M., 1992: Tropical cyclogenesis in the western North Pacific. NOAA Tech. Rep. NESDIS 61, 181 pp. [Available from NOAA/NESDIS, E/RA22, 5200 Auth Road, Washington, DC 20233.]

——, 2003: Environmental vertical wind shear with Hurricane Bertha (1996). *Wea. Forecasting,* **18,** 345–356.